Effect of Slag Tap Size on Gasification Performance and Heat Losses in a Quench-Type Coal Gasifier

Ting Wang and Armin Silaen
University of New Orleans
Energy Conversion & Conservation Center
New Orleans, Louisiana, USA

Heng-Wen Hsu and Cheng-Hsien Shen
Energy and Resources Laboratory
Industrial Technology Research Institute
Taiwan, R.O.C.

ABSTRACT

Operation of a quench-type coal gasifier has frequently encountered the problem of a clogged slag tap. The slag tap is located at the bottom of the gasifier allowing molten slag to flow down to the quenching water bath. The current design of the slag tap has an opening of 33% of the gasifier's inner diameter. The clogging problem can be temporarily resolved by employing a kerosene burner to melt the solidified slag. However, it is desirable to permanently resolve this problem by opening up the slag tap and/or directing the coal injector downward. There is a concerned that opening the slag tap wider would allow more heat losses and result in both reduced thermal efficiency and degraded gasification performance. Therefore, before conducting expensive hardware retrofits and tests, computer simulation to analyze several different options is employed. The complete 3-D Navier-Stokes equations are solved. The simulation models the gasification process with three global heterogeneous reactions and three homogeneous reactions, including volatile combustion.

The results show that the gas in the quenching section is almost stagnant. Opening up the slag tap only slightly increases flow motion in the quenching section. Temperature in the upper half of quenching section increases several hundred degrees but maintains the same in the lower half portion of the quenching section. This implies that radiation is the major heat transfer mode between the cold water bath and hot gas in the gasifer. Opening the slag tap increases shape factor and increases heat loss to the water bath. Unburned volatile fraction also increases as slag tap widens. There is always the concern that unburned volatile could be condensed into tar in the cooler downstream of gasifier during the cold-stream clean up process. Changing the injection direction from horizontal to 15 degrees downward does not make a noticeable difference to the gas temperature or gasification performance. The benefit of opening the slap tap wider by allowing slag to move successfully without clogging is compromised by increased heat losses, reduced gasification performance, downgraded syngas heating value, and increased unburned volatile matter. In this study, the overall gasification performance and syngas fuel heating values downgraded approximately 10% when slag tap opening widens from 2-inch to 6-inch in diameter.

1.0 INTRODUCTION

The Energy and Resources Laboratories of the Industrial Technology Research Institute (ITRI) constructed a demonstration gasifier [Hsu, et. al., 2003] in the Southern Taiwan city of Kaohsiung. The gasifier, shown in Fig. 1, is designed for a maximum load of two tons of coal per day. The gasifier is operated with oxygen-blown scheme. Coal powder is transported by nitrogen and feeds from the bottom. The hot gas flows upwards and exits from the top. A water spray device is installed on the top of the gasifier to adjust the H_2 or CO content of the syngas. If necessary, a water spray device is also used to control the exit gas temperature. Slag that forms on the inside wall flows to the bottom through a slag tap throat and is quenched in a water bath.

This facility is designed to convert pulverized coal and petroleum cokes into syngas at a pressure below 15 bars. The designed coal gasification efficiency under full-load operation is approximately 75% and carbon conversion exceeds 90%. The experimental system includes the following major sections: solids handling, solids feeding, gas feeding, gasification, syngas cooling, slag discharge, fines removal.

The solid feed materials include pulverized coal, petroleum cokes, and fluxing agents such as limestone. The feed materials are pulverized to a size distribution of greater than 70% by weight by passing through 200 mesh. The feed solids are discharged by the hoppers via rotary feeders and a screw conveyor, and are then transferred to the three feed injection vessels. The feed solids are discharged from the injection vessels by variable speed metering screws located at the bottom of the injection vessels. These screws are used to control the rate of the solids that are fed into the pipes of gasifier. The feed solids are mixed with oxygen and steam and are injected into the gasifier through three feed nozzles by a dense-phase pneumatic conveying system using high-pressure nitrogen.

The gasifier consists of a gasification section and a slag quench section. The gasification section is a single-

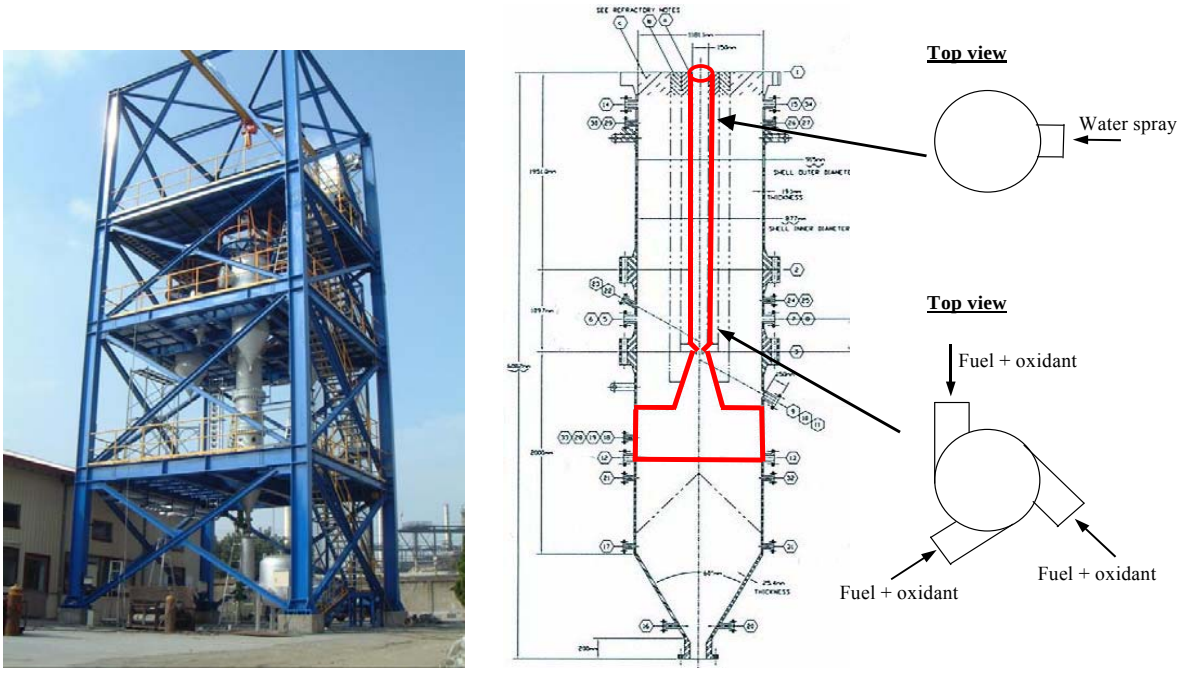

(a) (b)

Figure 1 (a) Actual facility and (b) schematic of the ITRI Gasifier. The computational domain is highlighted red.

stage, refractory-lined, entrained-flow reactor where the feed solids react with oxidants and steam to be converted into syngas. The molten slag generated from the gasification section flows down through slag tap opening located at the bottom of the gasification section and falls into the slag quench section for water quenching. The designed slag tap opening size is 33% of the gasifier inner diameter.

Unfortunately, with the current slag tap design, the problem of clogged slag tap is often encountered. The clogging problem can be temporarily resolved by employing a kerosene burner to melt the solidified slag. However resolving this problem permanently by opening up the slag tap and/or directing the coal injector downward is more desirable. There is a concern that opening the slag tap wider would allow more heat losses to the water bath and result in both reduced thermal efficiency and degraded gasification performance. Therefore, computational simulations are conducted to investigate the possibility of modifying the slag tap opening size or the fuel/oxidant injections direction to help avoid the clogged slag tap problem without adversely affecting the performance. This is one of the challenges between the scaling of larger and the smaller gasifiers. The slag tap opening of the larger gasifer can not be adequately scaled down to smaller gasifiers. Therefore, an independent study of slag tap opening size needs to be conducted for each different size of gasifier.

1.1 Gasification Process

The global chemical reactions of coal gasification [Smoot and Smith, 1985] can be generalized as below:

Heterogeneous (solid and gas) phase:

$C(s) + \frac{1}{2} O_2 \rightarrow CO$, $\Delta H°R = -110.5$ MJ/kmol (R1.1)

$C(s) + CO_2 \rightarrow 2CO$, $\Delta H°R = +172.0$ MJ/kmol (R1.2)
(Gasification,Boudouard reaction)

$C(s) + H_2O(g) \rightarrow CO + H_2$, $\Delta H°R = +131.4$ MJ/kmol
(Gasification) (R1.3)

$C + 2H_2 \rightarrow CH_4$ $\Delta H^oR = -87.4$ MJ/kmol
(Direct methanation) (R1.4)

Homogenous gas phase:

$CO + \frac{1}{2} O_2 \rightarrow CO_2$, $\Delta H°R = -283.1$ MJ/kmol (R1.5)

$CO + H2O(g) \rightarrow CO_2 + H_2$, $\Delta H°R = -41.0$ MJ/kmol
(Water-shift) (R1.6)

$CO + 3H_2 \rightarrow CH_4 + H_2O$, $\Delta H^o_R = -205.7$ MJ/kmol
(Methanation) (R1.7)

$VM + O_2 \rightarrow CO_2 + H_2O$ (R1.8)
(VM is assumed as $CH_{3.086}O_{0.131}$)

Reactions given in R1.1, R1.5, and R1.8 are three exothermic reactions that provide the complete energy for the gasification. Based on these global reactions, approximately 22% of the stoichiometric oxygen is required to provide sufficient energy for gasification

reactions. In real applications, 25~30% of the stoichiometric oxygen is provided to ensure high-efficient carbon conversion. Methanation (R1.4 and R1.7) is assumed to be negligible in this study, so it is not included in the computational model in this study. The volatile matters (VM) are assumed as $CH_{3.086}O_{0.131}$ which has a medium heating value. The ideal operation intends to burn the volatile but not chars, so all the carbon could be used for gasification, not for combustion.

Partial combustion occurs when the VM and coal mix with oxygen (R1.1 and 1.8). The energy released from (R1.1 and 1.8) also heats up any coal that has not burned. When the coal is heated without oxygen, it undergoes pyrolysis during which volatiles are released. At the same time, char gasification (R1.2) takes place and releases CO. If a significant amount of steam exists, gasification (R1.3) and water shift reaction (R1.6) occur and release H_2.

2.0 COMPUTATIONAL MODEL

The schematic of the ITRI gasifier is shown in Fig.1. The area highlighted by the red bold line is the computational domain considered for this study. The detailed computational model and associated equations have been documented in detail by Silaen and Wang [2005 and 2006]. Only the major procedures are outlined in this paper.

2.1 Physical Characteristics of the Model and Assumptions

The physical characteristics of the model are:

1. Three-dimensional
2. Buoyancy force and radiation are considered
3. Varying fluid properties
4. Impermeable walls

The following general assumptions are made in this study:

1. The flow is steady.
2. No-slip condition (zero velocity) is imposed on wall surfaces.
3. Chemical reaction is faster than the time scale of the turbulence eddies: eddy dissipation model is adopted.
4. Walls are insulated (i.e. adiabatic).
5. Slagging is not considered.

2.2 Governing Equations

The equations for conservation laws of mass, momentum, and energy are given as:

$$\nabla \cdot \left(\rho \vec{v}\right) = S_m \tag{1}$$

$$\nabla \cdot \left(\rho \vec{v}\vec{v}\right) = -\nabla p + \nabla \cdot \left(\overline{\overline{\tau}}\right) + \rho \vec{g} + \vec{F} \tag{2}$$

$$\nabla \cdot \left(\vec{v}\left(\rho E + p\right)\right) = \nabla \cdot \left(\lambda_{eff} \nabla T - \sum_j h_j \vec{J}_j + \left(\overline{\overline{\tau}}_{eff} \cdot \vec{v}\right)\right) + S_h \tag{3}$$

where λ_{eff} is the effective conductivity which include the molecular thermal conductivity(λ) and the turbulence conductivity λ_t. J_j is the flux of species j.

The stress tensor $\overline{\overline{\tau}}$ is given by

$$\overline{\overline{\tau}} = \mu\left[\left(\nabla \vec{v} + \nabla \vec{v}^T\right) - \frac{2}{3}\nabla \cdot \vec{v} I\right] \tag{4}$$

where μ is the molecular dynamic viscosity, I is the unit tensor, and the second term on the right-hand side is the effect of volume dilatation. The first three terms on the right-hand side of equation (3) represent heat transfer due to conduction, species diffusion, and viscous dissipation. S_h is a source term including the enthalpy formation from the chemical reaction of the species. The energy E is defined as

$$E = h - \frac{p}{\rho} + \frac{v^2}{2} \tag{5}$$

where h is the sensible enthalpy and for incompressible flow given as

$$h = \sum_j Y_j h_j + \frac{p}{\rho} \tag{6}$$

Y_j is the mass fraction of species j and

$$h = \int_{T_{ref}}^{T} c_{p,j} dT \tag{7}$$

where T_{ref} is the reference temperature set at 298.15 K.

2.3 Turbulence Model

The standard k-ε turbulence model is used in this simulation due to its suitability for a wide range of wall-bound and free-shear flows. The standard k-ε turbulence model is robust, economic for computation, and accurate for a wide range of turbulent flows. The turbulence kinetic energy, k, and its rate of dissipations, ε, are calculated from the equations from the paper by Lauder and Spalding [1972]. Both buoyancy and minor compressibility effects on the turbulence model are considered.

The turbulence models are valid for the turbulent core flows, i.e. the flow in the regions not in the immediate proximity of the wall. The flow very near the walls is affected by the presence of the walls. In the viscous sublayer, where the solution variables change most rapidly, is not solved in this study. Instead, wall functions, which are a collection of semi-empirical formulas and functions, are employed to connect the viscosity-affected region between the wall and the fully-turbulent region [Lauder and Spalding, 1974]. The wall functions consist of (i) laws-of-the-wall for mean

velocity and temperature (or other scalars) and (ii) formulas for near-wall turbulent quantities. The standard wall functions for velocity, temperature, and species are employed in this study. See Silaen and Wang [2005 and 2006] for details.

2.4 Radiation Model

The P-1 radiation model is used to calculate the flux of the radiation at the inside walls of the gasifier. The P-1 radiation model is the simplest case of the more general P-N radiation model that is based on the expansion of the radiation intensity I. The P-1 model requires only a little CPU demand and can easily be applied to various complicated geometries. It is suitable for applications where the optical thickness aL is large where "a" is the absorption coefficient, and L is the length scale of the domain. See FLUENT user guide for details [2005].

2.5 Combustion Model

The global reaction mechanism is modeled to involve the following chemical species: C, O_2, N_2, CO, CO_2, VM, H_2O and H_2 (see reactions R1.1 through R1.5). The experimental data shows methanation is insignificant in the studied gasifier, so reactions R1.6 and R1.7 are not included in the simulation. All of the species are assumed to mix in the molecular level. The chemical reactions inside the gasifier are modeled by calculating the transport and mixing of the chemical species by solving the conservation equations that describe convection, diffusion, and reaction of each component species. The general form of the transport equation for each species is

$$\frac{\partial}{\partial t}\left(\rho Y_i\right)+\nabla\cdot\left(\rho\vec{v}Y_i\right)=-\nabla\cdot\vec{J}_i+R_i \cdot \qquad (8)$$

R_i is the net rate of production of species i by chemical reaction. $\vec{J}_i$ is the diffusion flux of species i, which arises due to concentration gradients. Mass diffusion for laminar flows is given as

$$\vec{J}_i=-\left(\rho D_{i,m}+\frac{\mu_t}{Sc_t}\right)\nabla Y_i \qquad (9)$$

where $D_{i,m}$ is the laminar bidiffusional coefficient and Sc_t is the turbulent Schmidt number

In this study, the eddy-dissipation model is used. The assumption in this model is that the chemical reaction is faster than the time scale of the turbulence eddies. Thus, the reaction rate is determined by the turbulence mixing of the species. The reaction is assumed to occur instantaneously when the reactants meet. The sources term R_i in equation (8) is calculated using the eddy-dissipation model based on the work of Magnussen and Hjertager [1976]. The net rate of production or destruction of species i as the result of reaction r, $R_{i,r}$, is given by the smaller of the two expressions below

$$R_{i,r}=\nu'_{i,r}M_{i,r}A\rho\frac{\varepsilon}{k}\min_R\left(\frac{Y_R}{\nu'_{R,r}M_{w,R}}\right) \qquad (10)$$

and

$$R_{i,r}=\nu'_{i,r}M_{i,r}B\rho\frac{\varepsilon}{k}\left(\frac{\sum_P Y_P}{\sum_j^N \nu''_{j,r}M_{w,j}}\right) \qquad (11)$$

where $\nu'_{i,r}$ is the stoichiometric coefficient of reactant i in reaction r and $\nu''_{j,r}$ is stoichiometric coefficient of product j in reaction r.

In equations (10) and (11), the chemical reaction rate is governed by large-eddy mixing time scale, k/ε. The smaller of the two expressions, (10) and (11), is used because it is the limiting value that determines the reaction rate. In this study, the solid particles are assumed to be gasified instantaneously, so the eddy-dissipation model can be applied. This instantaneous solid-gasification approach will provide results between the finite-rate reaction approach and chemically equilibrium approach.

The procedure to solve the reactions is as follows:

1. The net local production or destruction of species *i* in each reaction (R1.1 to R1.5) is calculated by solving equations (10) and (11).
2. The smaller of these values is substituted into the corresponding species transport equation (8) to calculate the local species mass fraction, Y_i.
3. Y_i is then used to calculate the net enthalpy production of each reaction equation.
4. The net enthalpy production becomes the source term in energy equation (3) that affects the temperature distribution. In an endothermic process, the net enthalpy production is negative, which becomes a sink term in the energy equation.

2.6 Discrete Phase (Water Droplets)

When water spray is used to increase the hydrogen content in the syngas or to reduce the syngas temperature, the discrete phase of water droplets are computed separately by modeling each individual droplet's heat transfer, water vaporization, and water vapor mass transfer. The interactions among particles are not modeled. The discrete phase is formulated by the Langrangian approach.

Droplet Flow and Heat Transfer – Basically, the droplets in the airflow can encounter inertia and hydrodynamic drags. Because of the forces experienced by a droplet in a flow field, the droplet can be either accelerated or decelerated. The velocity change can be formulated by

$$m_p d\mathbf{v_p}/dt = \mathbf{F_d} + \mathbf{F_g} + \mathbf{F_o} \qquad (12)$$

where $\mathbf{F_d}$ is the drag of the fluid on the droplet and $\mathbf{F_g}$ is the gravity. $\mathbf{F_o}$ represents the other forces, and $\mathbf{v_p}$ is the droplet velocity (vector). Among the forces represented by F_o are typically included the "virtual mass" force, thermophoretic force, Brownian force, Saffman's lift force, etc.

Theoretically, evaporation occurs at two stages: (a) when the temperature is higher than the saturation temperature (based on local water vapor concentration), water evaporates from the droplet's surface, and the evaporation is controlled by the water vapor partial pressure until 100% relative humidity is achieved; and (b) when the boiling temperature (determined by the air-water mixture pressure) is reached, water continues to evaporate even though the relative humidity reaches 100%. After the droplet is evaporated due to either high temperature or low moisture partial pressure, the vapor diffuses into the main flow and is transported away. The rate of vaporization is governed by concentration difference between surface and air stream, and the corresponding mass change rate of the droplet can be given by,

$$\frac{dm_p}{dt} = \pi d^2 k_c (C_s - C_\infty) \tag{13}$$

where k_c is the mass transfer coefficient and C_s is the concentration of the vapor at the droplet surface, which is evaluated by assuming that the flow over the surface is saturated. C_∞ is the vapor concentration of the bulk flow, obtained by solving the transport equations. The values of k_c can be calculated from empirical correlations by [Ranz and Marshall, 1955]:

$$Sh_d = \frac{k_c d}{D} = 2.0 + 0.6 Re_d^{0.5} Sc^{0.33} \tag{14}$$

where Sh is the Sherwood number, Sc is the Schmidt number (defined as ν/D), D is the diffusion coefficient of vapor in the bulk flow. Re_d is the Reynolds number, defined as $u\nu/d$, u is the flow velocity.

When the droplet temperature reaches the boiling point, the following equation can be used to evaluate its evaporation rate [Kuo, 1985]:

$$\frac{dm_p}{dt} = \pi d^2 \left(\frac{\lambda}{d}\right)(2.0 + 0.46 Re_d^{0.5}) \ln\left(1 + c_p(T_\infty - T)/h_{fg}\right)/c_p \tag{15}$$

where λ is the heat conductivity of the gas/air, and h_{fg} is the droplet latent heat. c_p is the specific heat of the bulk flow.

The droplet temperature can also be changed due to heat transfer between droplets and the continuous phase. Without considering radiation heat transfer, the droplet's sensible heat change depends on the convective heat transfer and latent heat (h_{fg}), as shown in the following equation.

$$m_p c_p \frac{dT}{dt} = \pi d^2 h(T_\infty - T) + \frac{dm_p}{dt} h_{fg} \tag{16}$$

where the convective heat transfer coefficient (h) can be obtained with a similar empirical correlation to equation (14):

$$Nu_d = \frac{hd}{\lambda} = 2.0 + 0.6 Re_d^{0.5} Pr^{0.33} \tag{17}$$

where Nu is the Nusselt number, and Pr is the Prandtl number.

In the gasifier, the temperature of main flow will be above the water boiling temperature. Notice the characteristic velocity in Re_d is the relative velocity between the droplet and gas flow, which is usually small for droplets in micrometers. Therefore, Re_d is also very small. In addition, the term $c_p(T_\infty - T)/h_{fg}$ in equation (15) can be much smaller than 1 (0.04 in this study). By ignoring the term with Re and using $\ln(1+\delta) = \delta$, the approximate droplet evaporation time can be obtained as:

$$t = \frac{h_{fg} \rho d^2}{2\lambda (T_\infty - T)} \tag{18}$$

This equation can be used to design the location of the water spray to ensure that water can be fully evaporated before the gasifier exit.

Stochastic Particle Tracking - The effects of turbulence on the dispersion of droplets/particles is considered by using stochastic tracking. Basically, the droplet trajectories are calculated by using the instantaneous flow velocity ($\bar{u} + u'$) rather than the average velocity ($\bar{u}$). The velocity fluctuations are then given as:

$$u' = \varsigma\left(\overline{u'^2}\right)^{0.5} = \varsigma(2k/3)^{0.5} \tag{19}$$

where ζ is a normally distributed random number. This velocity will apply during the characteristic lifetime of the eddy (t_e), a time scale defined by either of the following equations:

$$t_e = -0.3k/\varepsilon \tag{20}$$

$$t_e = -0.15k/\varepsilon \log(r) \tag{21}$$

where r is a uniform distributed random number ranging from 0 to 1. In case the droplet slip velocity is so large that the time for the droplet to cross the eddy is shorter than the time defined above, the droplet eddy crossing time will be used, which is defined as:

$$t_{cross} = -t_p \ln[1 - L_e/(t_p|u - u_p|)] \tag{22}$$

where t_p is the particle relaxation time with $t_p = \rho_p d_p^2/(18\rho_g \nu_g)$, L_e is the eddy length scale, and $|u-u_p|$ is the magnitude of the relative velocity. After this time period, the instantaneous velocity will be updated with a new ζ value until a full trajectory is obtained. The random effect of the turbulence on the droplets can

predicted reasonably only if a sufficient number of trajectories are calculated. In this study, the trajectory number is chosen to be 25 and several test runs indicated that increasing this number does not make the result much different.

2.7 Inlet and Boundary Conditions

Indonesian coal is used as feedstock in this study. Its composition is given in Table 1 and the feed rates used are given in Table 2. The oxidant used is 95% O_2 and 5% N_2. Oxidant/coal feed rate used in Table 2 gives O/coal value of 0.64. The O/pure-Carbon ratio is 0.6 of the stoichiometric O/pure-Carbon ratio. Fig. 2 presents the boundary conditions used in this study.

Table 1 Composition of Indonesia Coal

	Weight %
Volatile	38.31%
H2O	8.25%
ash	3.90%
C	37.95%
H	2.68%
N	0.69%
S	0.31%
O	7.91%
Total, wt %	100.00%
HHV, kcal/kg	5690

Table 2 Feed rates used in the study

	Feed rate (kg/hr)
Coal	83.5
Steam	3.14
Oxidant	53.37
Transport nitrogen	24.05

2.8 Studied Cases

A total of four cases are investigated in this study as shown in Fig. 3. Case 1 is for the current slag tap opening which is 2 inches in diameter and is 33% of the gasifier's inner diameter (6 inches). Two other wider slag tap openings are also investigated with Case 2: 66% (4 inches) and Case 3: 100% (6 inches, i.e. no slag tap) of gasifier inner diameter. Cases 2 include two fuel injection arrangements: Case 2a has the current horizontal injection arrangement with an tangential angle of 45° while Case 2b injects fuel 15° downward plus an tangential angle of 45° intending to help further melt the slag near the slag tap throat to avoid clogging.

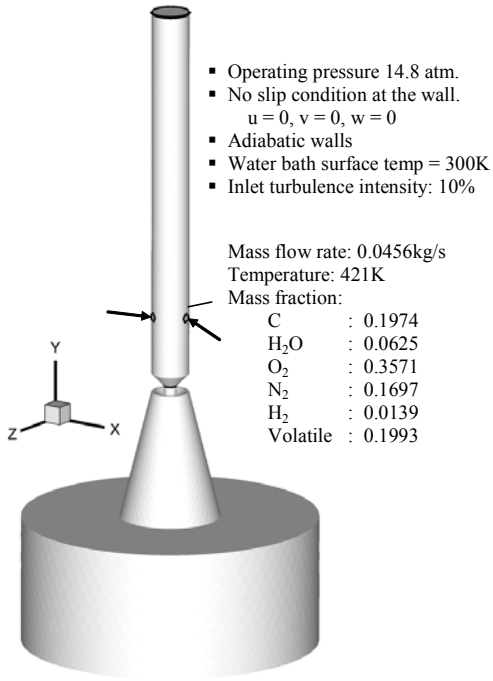

Figure 2 Boundary and inlet conditions

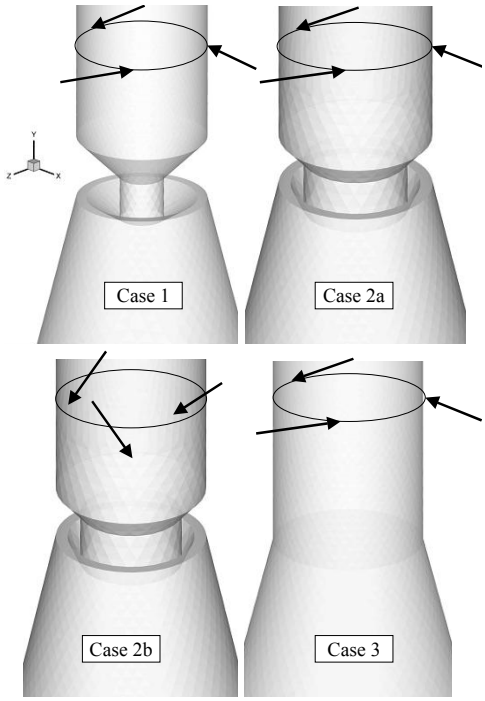

Figure 3 Four studied cases: (a) Case 1: 2 inch opening (b) Case 2a: 4-inch opening. (c) Case 2b: 4-inch opening, injection 15° downward (d) Case 3 6-inch opening (no slag tap).

The geometry and mesh are generated in the preprocessing tool, GAMBIT. The CFD solver used in this study is the commercial CFD code FLUENT

Version 6.2.16 [2005]. The simulation uses the segregated solver, which employs an implicit pressure-correction scheme. The SIMPLE algorithm is used to couple the pressure and velocity. Second order upwind scheme is selected for spatial discretization of the convective terms and species. Lagrangian trajectory calculations are employed for the dispersed phase of droplets. After obtaining an approximate flow field of the airflow, the droplet trajectories are calculated. At the same time, drag, heat and mass transfer between the droplets and the airflow is calculated. Iteration proceeds alternatively between the continuous and discrete phases. Ten iterations in the continuous phase are conducted between two iterations in the discrete phase. A cluster of 9-node parallel processor is used. It takes a clock-time of 9 hours to achieved convergence. The convergence criteria are $1x10^{-3}$ for continuity, $1x10^{-5}$ for energy, and $1x10^{-4}$ for radiation and all species.

3.0 RESULTS AND DISCUSSIONS

To evaluate the gasifier performance, four different indicators are defined in this study:

$$\text{Carbon conversion efficiency} \equiv 1 - \frac{\text{carbon at the exit}}{\text{raw carbon} + \text{recycled carbon}} \quad (23)$$

$$\text{Carbon fuel conversion efficiency} \equiv \frac{[\text{CO} + \text{CH}_4]_{\text{mole}}}{[\text{raw carbon}]_{\text{mole}}} \quad (24)$$

$$\text{Fuel conversion efficiency} \equiv \frac{[\text{H}_2 + \text{CO} + \text{CH}_4]_{\text{moles}}}{[\text{raw carbon} + \text{H}_2\text{O} + \text{O}_2]_{\text{moles}}} \quad (25)$$

$$\text{Gasification efficiency} \equiv \frac{[\text{H}_2 + \text{CO} + \text{CH}_4]_{\text{heating value}}}{[\text{coal}]_{\text{heating value}}} \quad (26)$$

The reasoning behind these definitions is explained in Wang et. al. (2006) and is not repeated here. The results are shown in Table 3. From the various conversion efficiency and syngas heating values, it can be clearly seen that increasing slag tap size from 2-inch to 6-inch diameter reduces the gasification performance and syngas heating value approximately 10%. The degradation of gasification performance is believed to be caused by increasing heat loss to cold water bath as slag tap opening widens. This is consistent with the concerns shared by the original gasifier's designer who designed the slag taps opening diameter to be 1/3 of the gasifier main chamber diameter to reduce heat losses. The increased heat loss with larger slag tap opening is supported by data in Table 4 that shows that heat loss increases 13.5% when the slag tap opens up from 2-inch to 6-inch in diameter.

Table 4 Heat loss to the water bath for four cases

	Heat flux, W/m^2
Case 1	579
Case 2a	614
Case 2b	616
Case 3	685

The velocity vectors on a vertical midplane of the gasifier for Case 1 (2-inch opening) in Fig. 4 show that the gas in the quench section is almost stagnant. Almost all of the gas that flows down (actually spirals down) from the gasification section is blocked by the constriction of the slag tap.

Table 3 Results for the cases studied.

Parameters	***Case 1***		***Case 2a***		***Case 2b***		***Case 3***	
Exit temperature, K	1342		1375		1360		1333	
Carbon fuel conversion efficiency, %	27%		26%		23%		16%	
Coal gasification conv. efficiency, %	31%		30%		30%		28%	
Fuel conversion efficiency, %	71%		69%		69%		65%	
Components at exit:	Mole fraction	Mole no. (mole)	Mole fraction	Mole no. (mole)	Mole fraction	Mole no. (mole)	Mole fraction	Mole no. (mole)
CO	9.4%	0.11	9.2%	0.11	7.8%	0.09	5.6%	0.07
H_2	39.2%	0.48	39.1%	0.46	40.0%	0.48	40.5%	0.47
CO_2	25.0%	0.30	26.5%	0.31	26.5%	0.32	29.0%	0.34
VM	14.1%	0.17	13.2%	0.16	13.5%	0.16	12.9%	0.15
H_2O	1.8%	0.02	1.5%	0.02	1.9%	0.02	2.7%	0.03
N_2	10.5%	0.13	10.5%	0.12	10.3%	0.12	10.2%	0.12
C	0.0%	0.00	0.0%	0.00	0.0%	0.00	0.0%	0.00
Heating value (MJ/kg)	7.9		7.6		7.7		7.2	

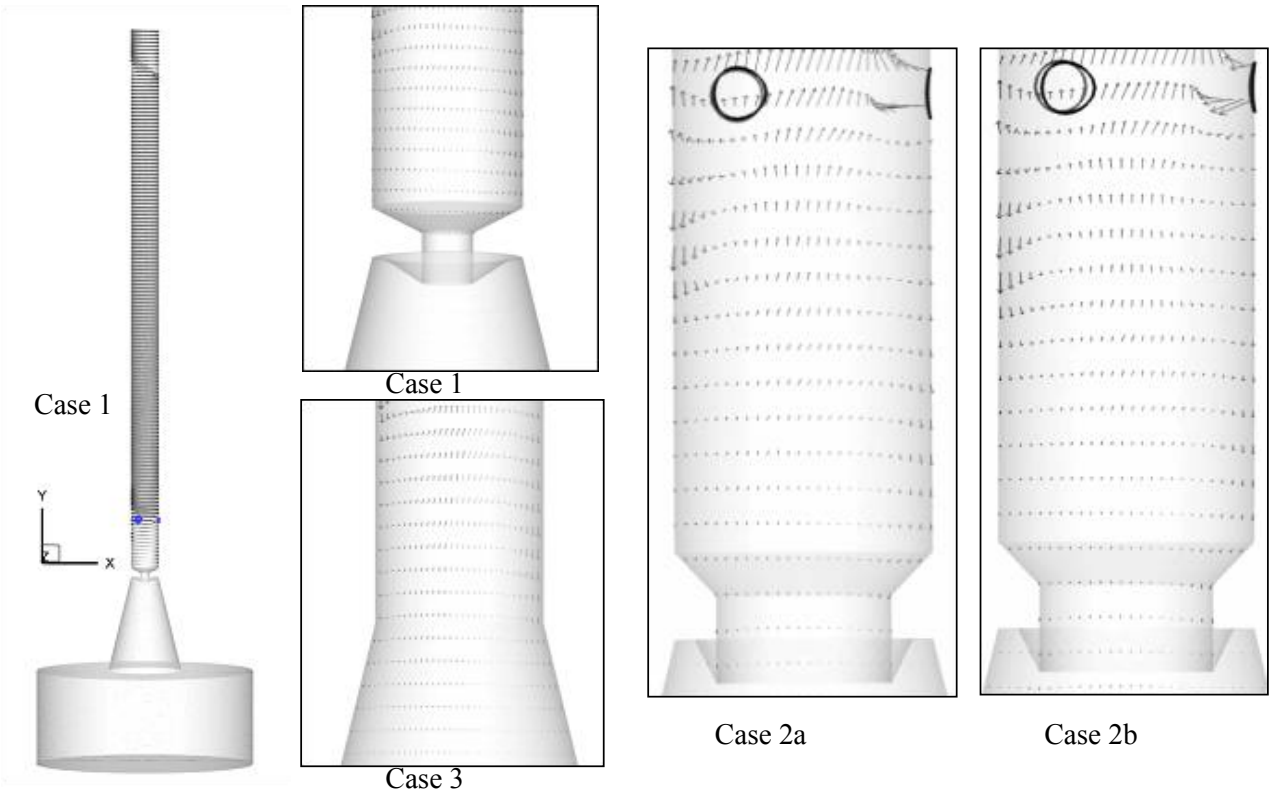

Fig. 4 Velocity vectors on vertical midplane of gasifier for four cases. Flow in the quenching section is almost stagnant for all cases.

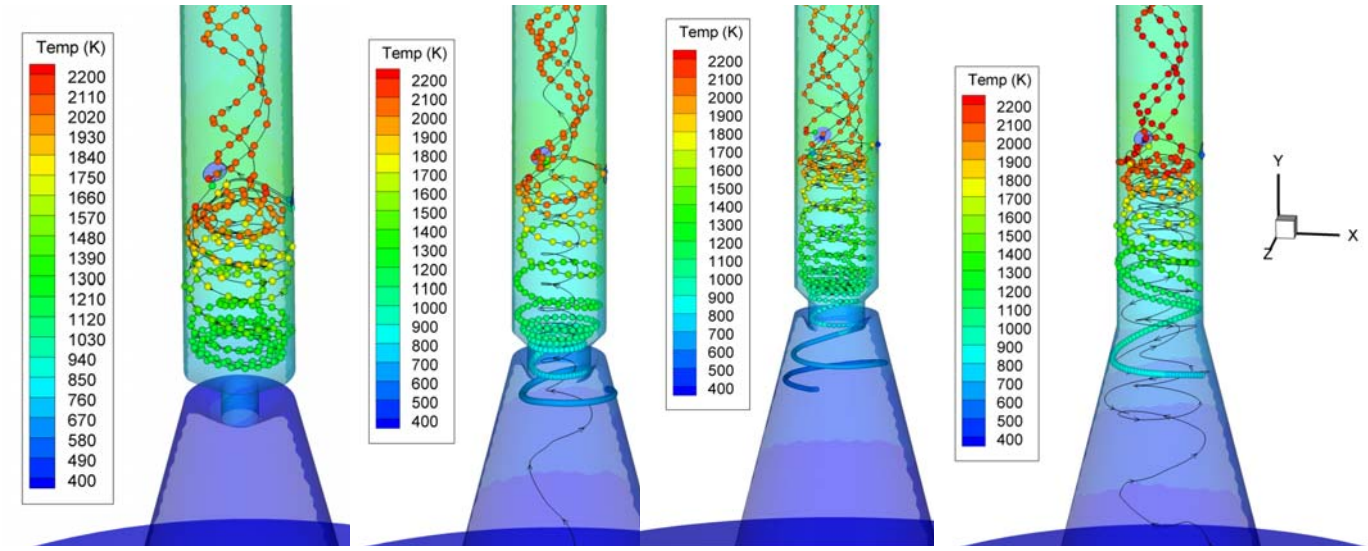

(a) Case 1 **(b) Case 2a** **(c) Case 2b** **(d) Case 3**

Figure 5 Flow pathline traces and temperature distributions for all cases. The background color is the translucent back wall temperature, not the gas temperature. The gas temperature is represented by the colors of the spheres. Minimal flow pathline traces are seen in the quench section.

Only a very small percentage of the gas spiraling through the slag tap throat and into the quench section. The spiraling down flow produces a core of upflowing breeze in the center of the downward spiraling column to maintain mass conservation, as can be seen in Fig. 5. As the opening is widened (Cases 2 and 3), more gas spirals down from the gasification section into the water bath section.

The effects of widening the slag tap opening on the gas temperature are observed in Fig. 6. Because of the small slag tap opening in Case 1, only a very small fraction of hot gas from the gasification section flows down through the slag tap throat. There is a large temperature difference across the slag tap. As the opening size is increased, more of the hot gas flows down through the slag tap opening and into the cold quenching region. Thus the gas temperature in the quenching section just below the slag tap (or upper part of the quenching section) becomes several hundred degrees higher as the slag tap opening size is increased. However lower half part of the quenching section maintains about the same temperature at near 350K irrespective of the slag tap opening sizes. Gas temperature in the gasification section does not show much variation between all cases. Since the flow in the quenching section is almost stagnant for all cases, the heat loss to the water bath is expected to be mainly transferred via radiation. Therefore, larger slag tap opening will induce a larger shape factor leading to larger heat transfer loss as previously shown in Table 4.

Gas composition plots in Fig. 7 show that gas compositions in the gasification section are almost identical for all slag tap opening sizes, except after the water spray. Water shift reaction occurs ($CO + H_2O \rightarrow CO_2 + H_2$) when the water is sprayed. As a result, a decreased in CO and an increase in both CO_2 and H_2 are observed. Among the four cases, Case 1 (smallest opening) has the highest CO content at the exit and the lowest CO_2 and H_2 contents. Case 3 (no tap), on the other hand, has the least amount of CO content and the highest CO_2 and H_2 content. Changing the injection direction from horizontal to 15 degrees downward (Case 2a to Case 2b) does not make noticeable difference to the gas temperature and compositions. Unburned volatile fraction seems to increase in Case 3 with no slag tap arrangement (wide open). There is the concern that unburned volatile could be condensed into tar in the cooler downstream of gasifier during the cold-stream clean up process. Therefore, it is essential to know the benefit as well as drawbacks of opening the slap tap wider. By allowing slag to move successfully without clogging, about 10% of gasification performance and syngas fuel heat value are compromised and lost. It should be noted that the present simulation has not considered the formation and flowing of molten slag layer, so the heat loss is over predicted. This is because, in the real situation, the slag layer will reduce the effective slag tap opening and hence, the radiation loss will be proportionally reduced.

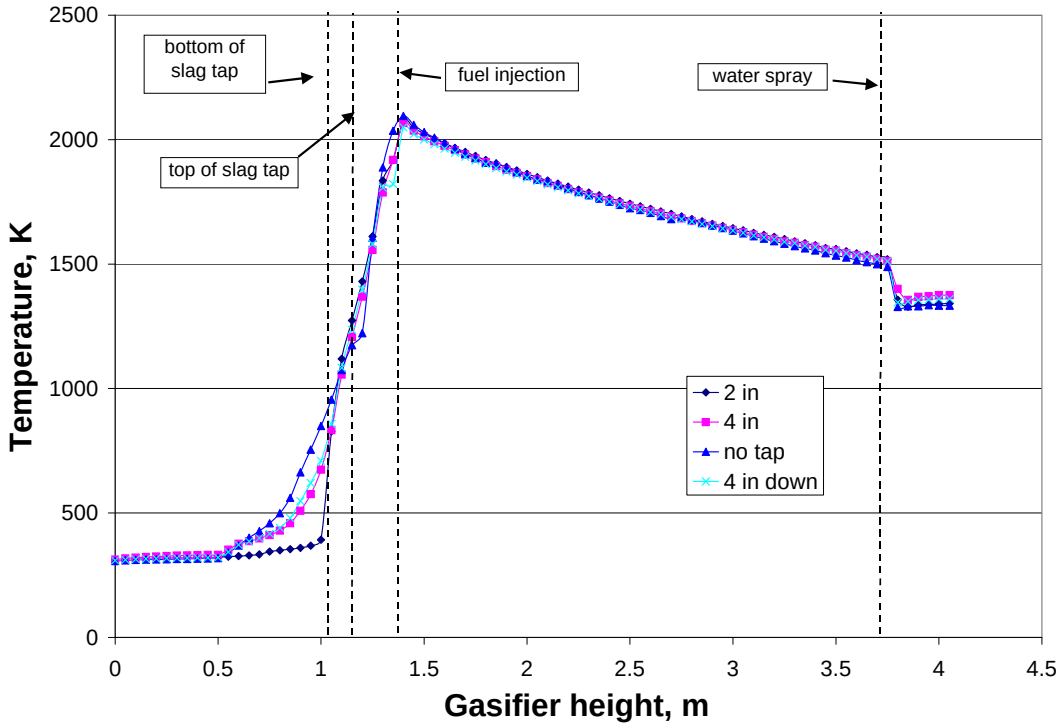

Fig. 6 Mass-weighted temperature average at different gasifier heights.

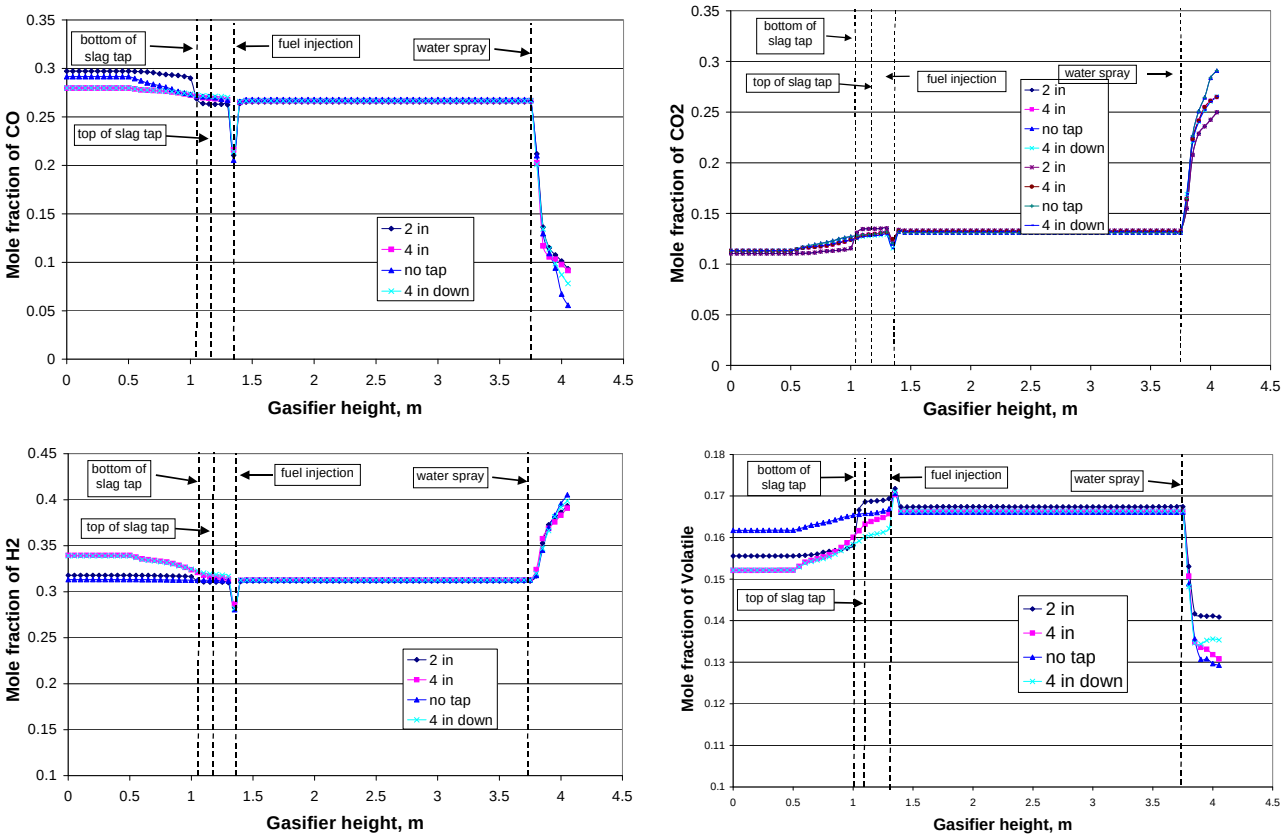

Fig. 7 Mass-weighted gas mole fractions at different gasifier heights.

4.0 CONCLUSIONS

Operation of a quench-type coal gasifier has frequently encountered the problem of clogged slag tap, especially for smaller gasifier. One possible means to avoid this problem is by widening the slag tap opening. The results show that the gas in the quenching section is almost stagnant. Opening up the slag tap only slightly increases flow motion in the quenching section. Temperature in the upper half of quenching section increases several hundred degrees, but it maintains the same in the lower half portion of the quenching section. This implies that radiation is the major heat transfer mode between the cold water bath and hot gas in the gasifer. Opening the slag tap increases shape factor and increases heat loss to the water bath. The overall gasification performance and syngas fuel heating values are downgraded approximately 10% when the slag tap opening widens from 2-inch to 6-inch in diameter. Unburned volatile fraction also increases as the slag tap widens. There is a concern that the increased unburned volatile could be quenched and condensed into tar in the cooler downstream of the gasifier during the cold-stream clean up process. Changing the injection direction from horizontal to 15 degrees downward does not make a noticeable difference to the gas temperature and gasification performance. The benefit of opening the slap tap wider by allowing slag to move successfully without clogging is compromised by increased heat losses, reduced gasification performance, downgraded syngas heating value, and increased unburned volatile matter.

5.0 ACKNOWLEDGEMENTS

The first two authors want to acknowledge the support from the Louisiana Governor's Energy Initiative, administered by the Louisiana Board of Regents via the Clean Power and Energy Research Consortium (CPERC). The ITRI coal gasification demonstration project is financed by the Bureau of Energy, Ministry of Economic Affairs, Taiwan.

6.0 REFERENCES

FLUENT 6.2.16 User's Guide, February 2005.

Hsu, H. W., Shieh, C.L., and Lo, M. C., "Application and Outlook for Clean Coal Technologies in Taiwan," Clean Energy Technology Division, Energy & Resource Laboratories, Industrial Technology Research Institute,

Taiwan, Proceedings of the20th Pittsburgh Coal Conference, 2003.
Kuo, K. Y., 1986, Principles of Combustion, John Wiley and Sons, New York.

Lauder, B.E., and Spalding, D.B., Lectures in Mathematical Modeling of Turbulence, Academic Press, London, England, 1972.

Lauder, B.E., and Spalding, D.B., The Numerical Computation of Turbulent Flows, Computer Methods in Applied Mechanics and Engineering, 3:269-289, 1974.

Magnussen, B.F., and Hjertager, On mathematical models of turbulent combustion with special emphasis on soot formation and combustion. In 16th Symp. (Int'l) on Combustion. The Combustion Institute, 1976.

Patankar, S.V., Numerical Heat Transfer and Fluid Flow, McGraw Hill, 1980.

Smoot, D.L., and Smith, P.J., Coal Combustion and Gasification, Plenum Press, 1985.

Ranz, W. E. and Marshall, W. R. Jr., 1952, "Evaporation from Drops, Part I and Part II," Chem. Eng. Prog., 48, pp. 141-146 and pp. 173-180.

Silaen, A. and Wang, T.," Simulation of Coal Gasification Process Inside a Two-Stage Gasifier," Paper007, Proceedings of the 22nd Pittsburgh Coal Conference, Pittsburgh, Pennsylvania, September 19-22, 2005.

Silaen, A. and Wang, T., "The Effect of Fuel Injection Directions on Coal Gasification Process Inside a Two-Stage Gasifier," Proceedings of the 23rd Pittsburgh Coal Conference, Pittsburgh, Pennsylvania, 2006.

Wang, T., Silaen, A., Hsu, H.W., and Lo, M.C., "Part-Load Simulations and Experiments of a Small Coal Gasifier," Proceedings of the 23rd Pittsburgh Coal Conference, Pittsburgh, Pennsylvania, 2006.